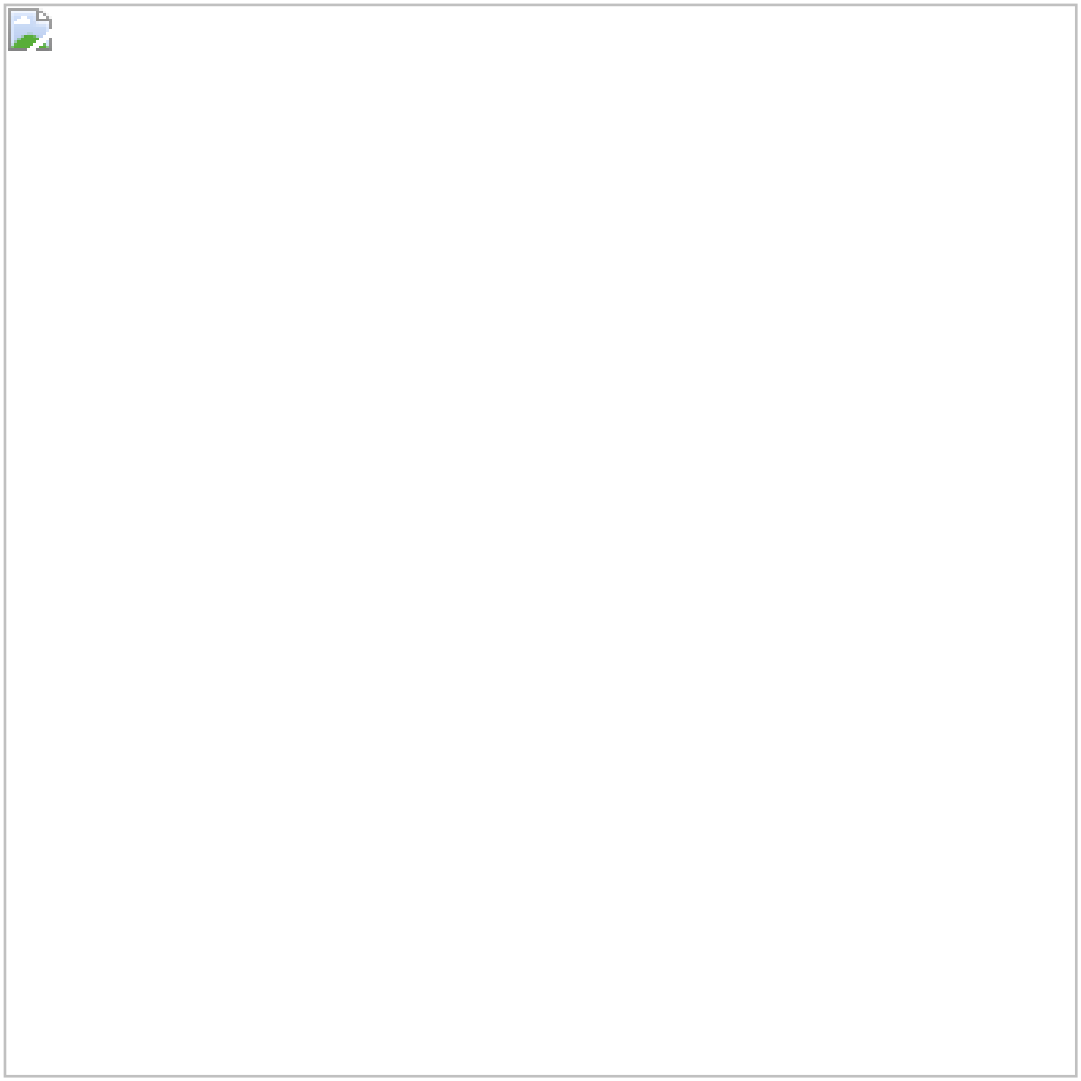

Role of Bcl2-like 10 (Bcl2l10) in Regulating Mouse Oocyte Maturation 1

Authors: Yoon, Se-Jin, Kim, Eun-Young, Kim, Yun Sun, Lee, Hyun-Seo, Kim, Kyeoung-Hwa, et al.

Source: Biology of Reproduction, 81(3) : 497-506

Published By: Society for the Study of Reproduction

URL: https://doi.org/10.1095/biolreprod.108.073759

BIOLOGY OF REPRODUCTION **81,** 497–506 (2009)
Published online before print 13 May 2009.
DOI 10.1095/biolreprod.108.073759

Role of Bcl2-like 10 (*Bcl2l10*) in Regulating Mouse Oocyte Maturation[1]

Se-Jin Yoon,[3,4] Eun-Young Kim,[4] Yun Sun Kim, Hyun-Seo Lee, Kyeoung-Hwa Kim, Jeehyeon Bae, and Kyung-Ah Lee[2]

Graduate School of Life Science and Biotechnology, Pochon CHA University College of Medicine, Seoul, Korea

ABSTRACT

Previously, we have shown that *Bcl2l10* is highly expressed in metaphase II (MII)-stage oocytes. The objective of this study was to characterize *Bcl2l10* expression in ovaries and to examine the function of *Bcl2l10* in oocyte maturation using RNA interference. *Bcl2l10* transcript expression was ovary and oocyte specific. *Bcl2l10* was highly expressed in oocytes and pronuclear-stage embryos; however, its expression decreased at the two-cell stage and dramatically disappeared thereafter. Microinjection of *Bcl2l10* double-stranded RNA into the cytoplasm of germinal vesicle oocytes resulted in a marked decrease in *Bcl2l10* mRNA and protein and metaphase I (MI) arrest (78.9%). Most MI-arrested oocytes exhibited abnormalities in their spindles and chromosome configurations. *Bcl2l10* RNA interference had an obvious effect on the activity of maturation-promoting factor but not on that of mitogen-activated protein kinase. We concluded that the role of *Bcl2l10* is strongly associated with oocyte maturation, especially at the MI–MII transition.

Bcl2l10, *MPF, oocyte maturation, RNA interference, spindle*

INTRODUCTION

Mammalian oocytes are arrested at the prophase of the first meiotic division, and with hormonal stimulation they undergo two successive asymmetric divisions during meiotic maturation to assure production of haploid oocytes that retain most of the maternal stores. In many species, oocytes accumulate RNAs and proteins during oogenesis not only for their development, but for their maturation, fertilization, and further embryonic development [1].

Previously, we have acquired list of the differentially expressed genes in germinal vesicle (GV) and metaphase II (MII) using an annealing control primer-PCR method to determine the molecular mechanism of meiotic arrest and meiotic resumption [2]. Although we disclose function of specific target genes one by one by using RNA interference (RNAi), it has been revealed that certain genes expressed in oocytes may regulate oocyte maturation [3], but certain genes may control embryo development rather than oocyte maturation [4].

We found that *Bcl2l10* mRNA is highly expressed in mouse MII-stage oocytes compared with GV oocytes [2]. BCL2L10, also called Diva (death inducer binding to *vBcl-2* and apoptosis-activating factor [APAF1]) was identified as a proapoptotic member of the *Bcl2* family that appeared not to require the BH3 domain for the induction of apoptosis [5]. Inconsistently, an antiapoptotic function of Boo (*Bcl2* homolog of ovary), the other name of Diva, and its exclusive expression in the ovaries and epididymis but not in the testes were reported in the mouse [6].

In addition to these contradictory, proapoptotic vs. antiapoptotic results regarding the role of BCL2L10 in apoptosis in granulosa cells, it has been demonstrated that BCL2L10 may play a role in Huntington-interacting protein 1-related (HIP1R) protein-mediated endocytosis and actin machinery [7]. Therefore, BCL2L10 may have different roles in the oocytes, and the present study was conducted to elucidate the roles of *Bcl2l10* in the mouse oocytes.

MATERIALS AND METHODS

Animals

All C57BL/6 mice were obtained from Koatech (Pyeoungtack, Korea) and were mated to male mice of the same strain in the breeding facility at the CHA Stem Cell Institute of Pochon CHA University to produce embryos. All procedures described in the present study were reviewed and approved by the University of Science Institutional Animal Care and Use Committee and were performed in accordance with the Guiding Principles for the Care and Use of Laboratory Animals.

Collection of Oocytes, Follicular Cells, and Embryos

Secondary follicles were mechanically isolated from 2-wk-old female C57BL/6 mice, and oocytes were separated from granulosa cells (GCs) by puncturing follicles with a needle. Collection of GV and MII oocytes and embryos at various stages was performed as described previously [3]. Cumulus cells (CCs) were removed from the oocytes using a fine-bore pipette. Mural GCs were recovered from preovulatory follicles. Isolated oocytes, embryos, CCs, and GCs were snap frozen and stored at −70°C for RNA isolation.

Reverse Transcription PCR

To confirm the cellular localization of *Bcl2l10* mRNA, RT-PCR analysis was performed on the isolated oocytes, CCs, and GCs from secondary or preovulatory follicles using *Bcl2l10*-specific primers that amplified a 551-bp amplicon (Fig. 1). Oocyte-specific mRNA expression was confirmed using murine *Gdf9*-specific primers, because *Gdf9* is known to be an oocyte-specific marker [8]. Sequences of the primers used are summarized in Table 1. To determine the expression of *Bcl2l10* mRNA during oocyte maturation and embryo development, an equivalent amount of single oocyte or embryo cDNA was used for real-time PCR analysis.

Northern Blot Analysis

Complementary DNA for *Bcl2l10* was synthesized from total RNA obtained from 4-wk-old mouse ovaries using *Bcl2l10*-specific primers,

[1]Supported by the Korea Research Foundation grant KRF-2006-311-E00067, funded by the Korean government (MOEHRD, Basic Research Promotion Fund).
[2]Correspondence: Kyung-Ah Lee, Graduate School of Life Science and Biotechnology, Pochon CHA University College of Medicine, 606-13 Yeoksam-1-dong, Gangnam-gu, Seoul 135-081, Korea.
FAX: 822 563 2028; e-mail: leeka@ovary.co.kr
[3]Current address: Department of Genetics, Stanford University School of Medicine, Stanford, CA 94305.
[4]These authors contributed equally to this work.

Received: 26 September 2008.
First decision: 16 October 2008.
Accepted: 22 April 2009.

eISSN: 1259-7268 http://www.biolreprod.org
ISSN: 0006-3363

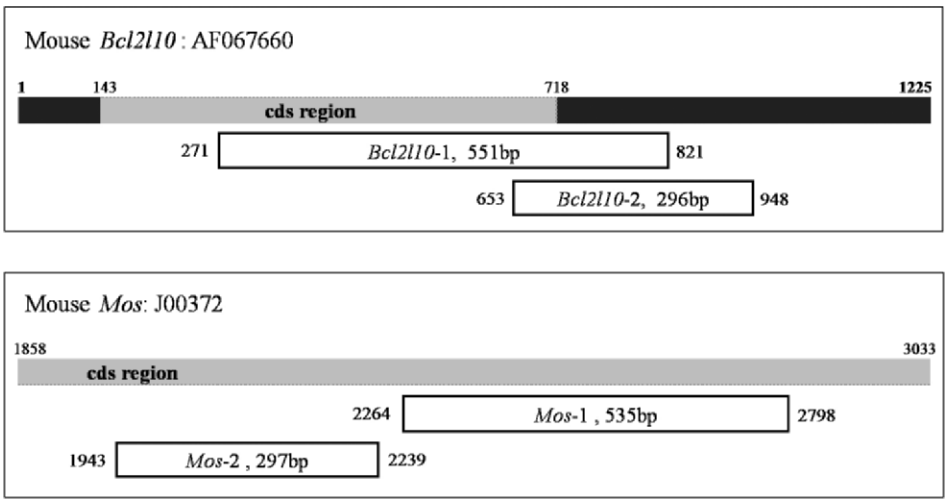

FIG. 1. Schematic diagram of mouse *Bcl2l10* (AF067660) gene showing the different locations of PCR-amplified products used for preparing *Bcl2l10* dsRNA (*Bcl2l10*-1) and confirming knockdown of endogenous *Bcl2l10* mRNA (*Bcl2l10*-2). The same is shown for the case of mouse *Mos* (J00372).

Bcl2l10-1, as shown in Table 1. A 551-bp fragment of *Bcl2l10* cDNA was radiolabeled with [^{32}P]-dCTP and used as a probe for hybridization as described previously [9].

Western Blot Analysis

For Western blot analysis, 20 μg per lane of the protein extract was subjected to 12% SDS-PAGE and transferred onto a polyvinylidene difluoride (PVDF) membrane (Immobilon-P; Millipore, Bedford, MA). The membranes were first incubated for 1 h in Tris-buffered saline-Tween (TBS-T; 0.1% Tween-20) containing 5% skim milk as a blocking agent. The blocked membranes were then incubated overnight with the primary antibody for BCL2L10 (1:200; sc-8739; Santa Cruz Biotechnology, Santa Cruz, CA) and mouse monoclonal anti-β-tubulin antibody (1:500; sc-8035; Santa Cruz Biotechnology) in TBS-T containing 3% bovine serum albumin (BSA; Sigma). After incubation, the membranes were incubated with horseradish peroxidase-conjugated anti-goat or anti-mouse secondary antibody, respectively, for 1 h. The blot was visualized using the Enhanced Chemiluminescence detection system (Santa Cruz Biotechnology).

In Situ Hybridization

Ovaries from 2- to 4-wk-old mice were fixed in 4% paraformaldehyde in PBS overnight at 4°C. Paraffin-embedded ovarian tissues were cut into 5-μm sections and mounted onto positively charged slides (ProbeOn Plus; Fisher Scientific, Pittsburgh, PA). Digoxigenin (DIG)-labeled *Bcl2l10* riboprobes were synthesized from a 551-bp fragment of *Bcl2l10* cDNA using an in vitro transcription kit (Promega, Madison, WI). Hybridization with a DIG-labeled antisense *Bcl2l10* probe was performed as described previously [9].

Quantitative Real-Time RT-PCR Analysis

Quantitative real-time RT-PCR analysis was also accomplished as described previously [3]. Reverse transcription was conducted at 42°C for 60 min, and the reaction was terminated by incubation at 94°C for 2 min. To measure the amount of *Bcl2l10* mRNA in a single oocyte or embryo, quantitative real-time RT-PCR analysis was performed using an iCycler (Bio-Rad, Hercules, CA). The template was amplified by 40 cycles of denaturation at 95°C for 40 sec, annealing at 60°C for 40 sec, and extension at 72°C for 40 sec. At the completion of the PCR, we monitored fluorescence continuously while slowly heating the samples from 60°C to 95°C at 0.5°C intervals, producing melting curves to identify any nonspecific products. Quantitation of gene amplification was made by determining the cycle threshold (C_T) based on the fluorescence detected within the geometric region of the semi-log amplification plot. Relative quantitation of target gene expression was evaluated using the comparative C_T method, and the experiments were repeated at least three times using different sets of oocytes and embryos.

RNAi for Bcl2l10

To determine the possible role of *Bcl2l10* in oocyte maturation, production of *Bcl2l10* double-stranded RNA (dsRNA) and RNAi by

TABLE 1. Sequences of oligonucleotide primers used in this study, their annealing temperatures (AT), and expected RT-PCR product sizes.

Gene*	GenBank accession no.	Oligonucleotide sequences†	AT (°C)	Size (bp)
Bcl2l10-1	AF067660	F: 5′-CTCTGTGACTAGGCAGATCC-3′ R: 5′-GTCTCTAGGCTGGAGGACTT-3′	60	551
Bcl2l10-2	AF067660	F: 5′-CTGATTCAGGCTTTTCTGTC-3′ R: 5′-CGTTTTCTGAAGTTCTCTGG-3′	60	296
Mos-1	J00372	F: 5′-CCATCAAGCAAGTAAACAAG-3′ R: 5′-AGGGTGATTCCAAAAGAGTA-3′	60	535
Mos-2	J00372	F: 5′-TGGCTGTTCCTACTCATTTC-3′ R: 5′-CTTTATACACCGAGCCAAAC-3′	60	297
Rn18s	J00623	F: 5′-GCTTGCGTTGATTAAGTCCC-3′ R: 5′-AGTTCGACCGTCTTCTCAGC-3′	60	139
Gapdh	BC092294	F: 5′-ACCACAGTCCATGCCATCAC-3′ R: 5′-TCCACCACCCTGTTGCTGTA-3′	60	451
Gdf9	NM_008110	F: 5′-GGTTCTATCTGATAGGCGAGG-3′ R: 5′-GGGGCTGAAGGAGGGAGG-3′	60	446
H1foo	NM_138311	F: 5′-GCGAAACCGAAAGAGGTCAGAA-3′ R: 5′-TGGAGGAGGTCTTGGGAAGTAA-3′	60	377
Plat	NM_008872	F: 5′-CATGGGCAAGAGTTACACAG-3′ R: 5′-CAGAGAAGAATGGAGACGAT-3′	60	650

* 1 indicates primer used for preparation of dsRNA and 2 indicates primer used for confirming knockdown of endogenous mRNA expression after RNAi.
† F, forward; R, reverse.

microinjection was performed as described previously [3]. To generate a template for *Bcl2l10* RNA transcription in vitro, 2 μg of total RNA from adult murine ovaries was reverse transcribed, the 551-bp PCR product amplified with the *Bcl2l10*-specific primers (AF 067660, 271–821) was run on a 1.5% agarose gel, and the cDNA fragment was cloned into a pGEM T-easy vector (Promega). Equimolar quantities of sense and antisense RNA were mixed and incubated in a single tube at 75°C for 5 min, then cooled to room temperature for 3 h. To avoid the presence of contaminant single-stranded cRNA in the dsRNA samples, the samples were treated with 1 μg/ml RNase A (Ambion) for 30 min at 37°C. The dsRNA was then subjected to a phenol-chloroform extraction, and the formation of dsRNA was confirmed by gel electrophoresis.

Double-stranded RNA for *Bcl2l10* was microinjected into the cytoplasm of mouse GV oocytes, as described previously [3]. Briefly, GV oocytes were microinjected with each dsRNA in M2 medium (Sigma) containing 0.2 mM 3-isobutyl-1-metyl-xanthine (IBMX; Sigma). An injection pipette containing dsRNA solution was inserted into the cytoplasm of an oocyte, and 10 pl of dsRNA (2.0 μg/μl) was microinjected using a constant-flow system (Transjector; Eppendorf, Hamburg, Germany). To assess injection damage, oocytes were injected with elution buffer alone and used as sham controls. Germinal vesicle oocytes in each group were cultured in M16 medium (Sigma) containing 3 mg/ml BSA (Sigma) or in M16 containing 0.2 mM IBMX for 8 h after RNAi, followed by culture in the plain M16 in a 5% CO_2 incubator at 37°C for 16 h according to experimental design. The meiotic status of oocytes was measured after 16 h. Oocytes without GV or a polar body (MII) were scored as metaphase I (MI). To determine the selective inhibition of *Bcl2l10*, *Mos* RNAi, a gene with a known RNAi effect, was used as an injection control [9, 10].

Confirmation of *Bcl2l10*-specific inhibition was performed by RT-PCR with primer set *Bcl2l10*-2, different from that used for *Bcl2l10* dsRNA production, to generate a 296-bp PCR product (Fig. 1 and Table 1). Messenger RNA from 5 to 10 oocytes was isolated using the Dynabeads mRNA Direct Kit (Dynal), and single-oocyte equivalents were used as templates for PCR amplification. The expression of other genes of interest was also measured after *Bcl2l10* RNAi. A list of these genes and primers is summarized in Table 1.

Dual Kinase Activity Assay

Changes in maturation-promoting factor (MPF) and mitogen-activated protein kinase (MAPK) activities were measured by examining the amount of phosphorylation of histone H1 and myelin basic protein (MBP) concurrently in one oocyte, as described previously [4]. Oocytes were washed in Dulbecco PBS containing 0.1% polyvinyl alcohol (PBS-PVA) and transferred into a tube in 1 μl of 0.1% PBS-PVA. Each sample contained one oocyte for double assay of MPF and MAPK and 4 μl of ice-cold extraction buffer (80 mM β-glycerophosphate, 25 mM Hepes [pH 7.2], 20 mM ethylene glycol tetraacetic acid, 15 mM $MgCl_2$, 1 mM dithiothreitol, 1 mM 4-amidinophehylmethane-sulfonyl fluoride hydrochloride (APMSF), 0.1 mM Na_3VO_4, 1 μg/μl leupeptin, and 1 μg/μl aprotinin). The samples were frozen and thawed; added to 5 μl of kinase buffer, 0.3 μCi/μl γ-[^{32}P]dATP (250 μCi per 25 μl; Amersham Pharmacia Biotech, Buckinghamshire, U.K.), and 5 μl of substrate solution; and incubated for 20 min at 37°C. The reaction was terminated by addition of 5 μl of 4× SDS sample buffer and boiling for 5 min. The labeled MBP and histone H1 were separated by SDS-PAGE (15% gel), and the gels were analyzed by autoradiography.

Noninvasive Examination of the Spindle Structure

Spindle structure observations of living oocytes were performed using the LC Pol-Scope optics and controller system, combined with a computerized image analysis system (Oosight Meta Imaging System; CRI Inc.).

Immunofluorescence Staining

Immunofluorescence staining for α-tubulin and DNA was accomplished as described previously [4]. Denuded oocytes were placed in PBS-PVA, 4% paraformaldehyde, and 0.2% Triton X-100, and then fixed for 40 min at room temperature. Fixed oocytes were washed three times in PBS-PVA for 10 min each and stored overnight in 1% BSA-supplemented PBS-PVA (BSA-PBS-PVA). Oocytes were blocked with 3% BSA-PBS-PVA for 1 h and incubated with the mouse monoclonal anti-α-tubulin antibody (1:100; sc-8035; Santa Cruz Biotechnology) at 4°C overnight. After washing, oocytes were incubated with fluorescein isothiocyanate-conjugated anti-mouse immunoglobulin G (1:40; Sigma) for 1 h at room temperature, and DNA was counterstained with propidium iodide (Sigma).

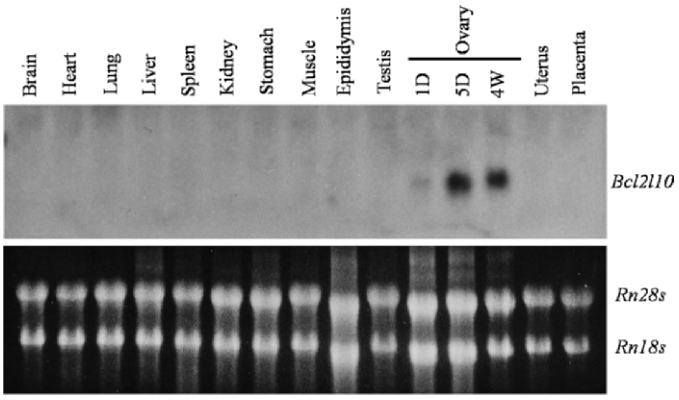

FIG. 2. Northern blot analysis of mouse *Bcl2l10* mRNA in various tissue types. Total RNA was extracted from multiple mouse tissues (20 μg per lane) as indicated with *Rn18s* and *Rn28s*. 1D, neonatal 1-day-old ovary; 5D, neonatal 5-day-old ovary; 4W, 4-wk-old ovary.

Aceto-orcein Staining

Oocytes were fixed in acetomethanol (acetic acid:methanol, 1:3) solution for 24 h at 4°C. Fixed oocytes were transferred to a microscope slide, and a clean coverslip (18-mm square) was placed over the top. A drop of aceto-orcein solution (1% orcein, 45% acetic acid) was placed, followed by incubation for 2–3 min and observation of chromosomes.

Oocyte Dot Blot

Oocyte dot blotting was accomplished as described previously [4]. Oocyte lysates were made and loaded onto a Hybond-P PVDF membrane (Amersham Biosciences), and the remaining procedures of dot blotting were the same as those of Western blotting. Expressed protein levels were quantified by measuring the intensity of the area for each dot using Bio 1D software (Vilber Lourmat), and the values were normalized by that of the α-tubulin dot and expressed as a percentage in comparison to that of control oocytes.

Statistical Analysis

Each experiment was repeated at least three times. The data are presented as mean ± SEM and were evaluated using a one-way ANOVA and log linear model. A value of $P < 0.05$ was considered to be statistically significant.

RESULTS

Expression of Bcl2l10 *Transcripts and Protein*

To evaluate the overall expression of *Bcl2l10* mRNA, Northern blotting was performed in various mouse tissues. Hybridization with a *Bcl2l10* probe revealed a single, prominent transcript of approximately 1.2 kb, which was found only in ovarian RNA and was undetectable in other tissues (Fig. 2). The expression was almost negative in neonatal 1-day-old ovaries that consisted mainly of primordial follicles, whereas it was clearly observed in postnatal 5-day-old ovaries that contained many growing follicles with more cuboidal follicular cells [9].

The localization of the *Bcl2l10* transcript in mouse ovaries was determined by in situ hybridization (Fig. 3, A–D). *Bcl2l10* mRNA expression was found mainly in the cytoplasm of preantral and antral follicular oocytes (Fig. 3, A–C). To verify this oocyte-specific expression, we performed RT-PCR using isolated oocytes, CCs, and GCs (Fig. 3E). To assess the expression pattern of *Bcl2l10* mRNA in oocyte maturation and the development of preimplantation embryos, real-time RT-PCR analysis was performed using cDNAs equivalent to single oocyte or single embryo. *Bcl2l10* was highly expressed in the GV-, MII-, and pronuclear (PN)-stage embryos, but expression

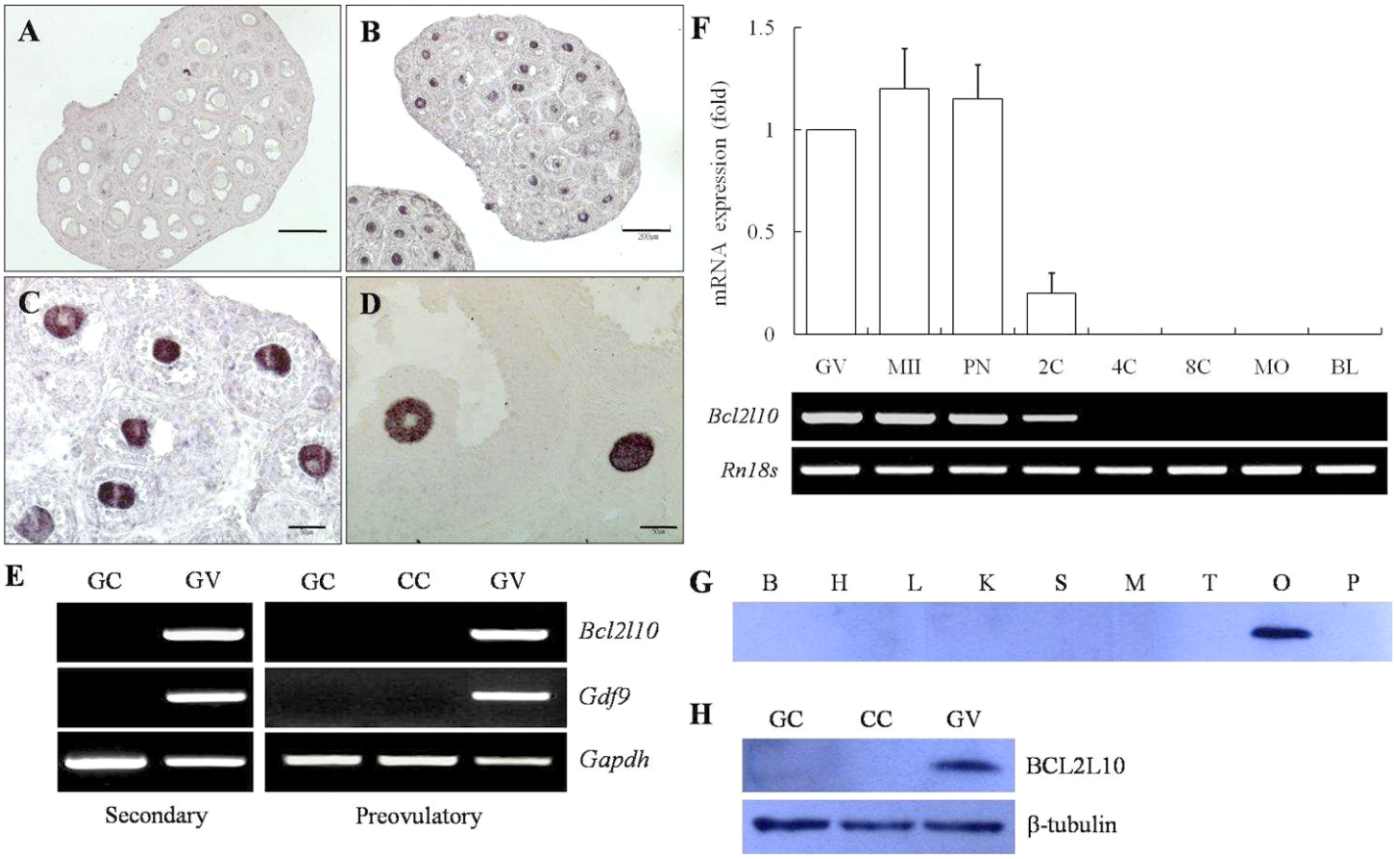

FIG. 3. Expression of *Bcl2l10* mRNA in murine ovaries. **A**–**D**) In situ hybridization of *Bcl2l10* mRNA. The mRNA expression of *Bcl2l10* is oocyte specific at all stages of follicular development except in primordial follicles. **A**) Negative control. **B** and **C**) Expression in oocytes in 2-wk-old ovaries. **D**) Expression in oocytes in equine chorionic gonadotropin-treated, 4-wk-old ovary. Bars = 200 μm (**A** and **B**) and 50 μm (**C** and **D**). **E**) Confirmation of oocyte-specific *Bcl2l10* mRNA using RT-PCR analysis. Preantral secondary follicles were isolated from 14-day-old ovaries, and GV-stage oocytes and GCs were mechanically isolated. Mural GCs and cumulus-oocyte complexes from preovulatory follicles were collected from 4-wk-old ovaries before oocytes (GV) and CCs were isolated using a fine-bore glass micropipette. *Gdf9* mRNA was used as a marker for oocyte-specific expression, and *Gapdh* was used as an internal control. **F**) Quantitative real-time RT-PCR of *Bcl2l10* mRNA in oocytes and embryos. The mRNAs isolated from oocytes and at various embryonic stages were reverse transcribed. For the PCR reaction, cDNA from a single oocyte or an embryo equivalent was used as a template for amplification. The expression level was calculated from the C_T values, and the mRNA ratio (arbitrary units) was calculated with respect to that of GV oocytes. Experiments were repeated at least three times, and data are expressed as the mean ± SEM. GV, GV-stage oocyte; MII, MII-stage oocyte; PN, pronucleus one-cell zygote; 2C, two-cell stage; 4C, four-cell stage; 8C, eight-cell stage; MO, morula stage; BL, blastocyst-stage embryo. **G** and **H**) Western blot analysis for BCL2L10 protein expression. Total protein (20 μg) from various mouse tissue types was electrophoresed and probed with an anti-BCL2L10 antibody. B, brain; H, heart; L, liver; K, kidney; S, stomach; M, muscle; T, testis; O, ovary; P, placenta. **H**) Protein lysates of GCs from 50 preovulatory follicles, CCs from 100 cumulus-oocyte complexes, and 200 GV oocytes (GVs) were loaded into each lane. β-Tubulin was used as a loading control.

dramatically decreased at the two-cell stage and was no longer detected at the four-cell stage and beyond (Fig. 3F).

Western blot analysis confirmed that BCL2L10 protein expression was ovary specific (Fig. 3G). BCL2L10 protein expression was also oocyte specific and negative in CCs and GCs (Fig. 3H), which was consistent with the results of the RT-PCR (Fig. 3E).

TABLE 2. In vitro maturation of mouse oocytes after *Bcl2l10* RNAi.

Treatment	No. of oocytes (%)			
	Total	Germinal vesicle (GV)	Metaphase I (MI)	Metaphase II (MII)
Control	178	2 (0.9)	32 (17.6)	144 (81.5)
Buffer	171	2 (3.2)	36 (16.2)	133 (80.6)
Bcl2l10 dsRNA	213	2 (1.0)	166 (78.9)*	45 (19.1)*

* Values are statistical significance at $P < 0.05$.

Bcl2l10 *RNAi in GV Oocytes and In Vitro Maturation*

To determine the roles played by *Bcl2l10* in oocyte maturation, RNAi was performed at the GV stage. Figure 4A depicts the constitutive expression of *Bcl2l10* mRNA during normal oocyte maturation in vitro, and Figure 4B shows the *Bcl2l10* dsRNA constructed in the laboratory. After the microinjection of *Bcl2l10* dsRNA into the cytoplasm of GV oocytes, the maturation rate to MII stage (19.1%) was significantly reduced compared with that of oocytes in control (81.5%) or buffer-injected (80.6%) groups (Table 2). Most of the oocytes arrested at the MI stage (78.9%) after *Bcl2l10* RNAi (Fig. 4C). *Bcl2l10* RNAi reduced endogenous *Bcl2l10* expression in MI and MII oocytes without effects on the expression of sequentially unrelated genes, such as *Mos* and *H1foo*, an oocyte-specific housekeeping histone gene (Fig. 4D). This finding suggests that the knockdown of *Bcl2l10* expression by RNAi was sequence specific.

In addition to using a buffer injection as sham control for microinjection, we performed *Mos* RNAi as control to validate

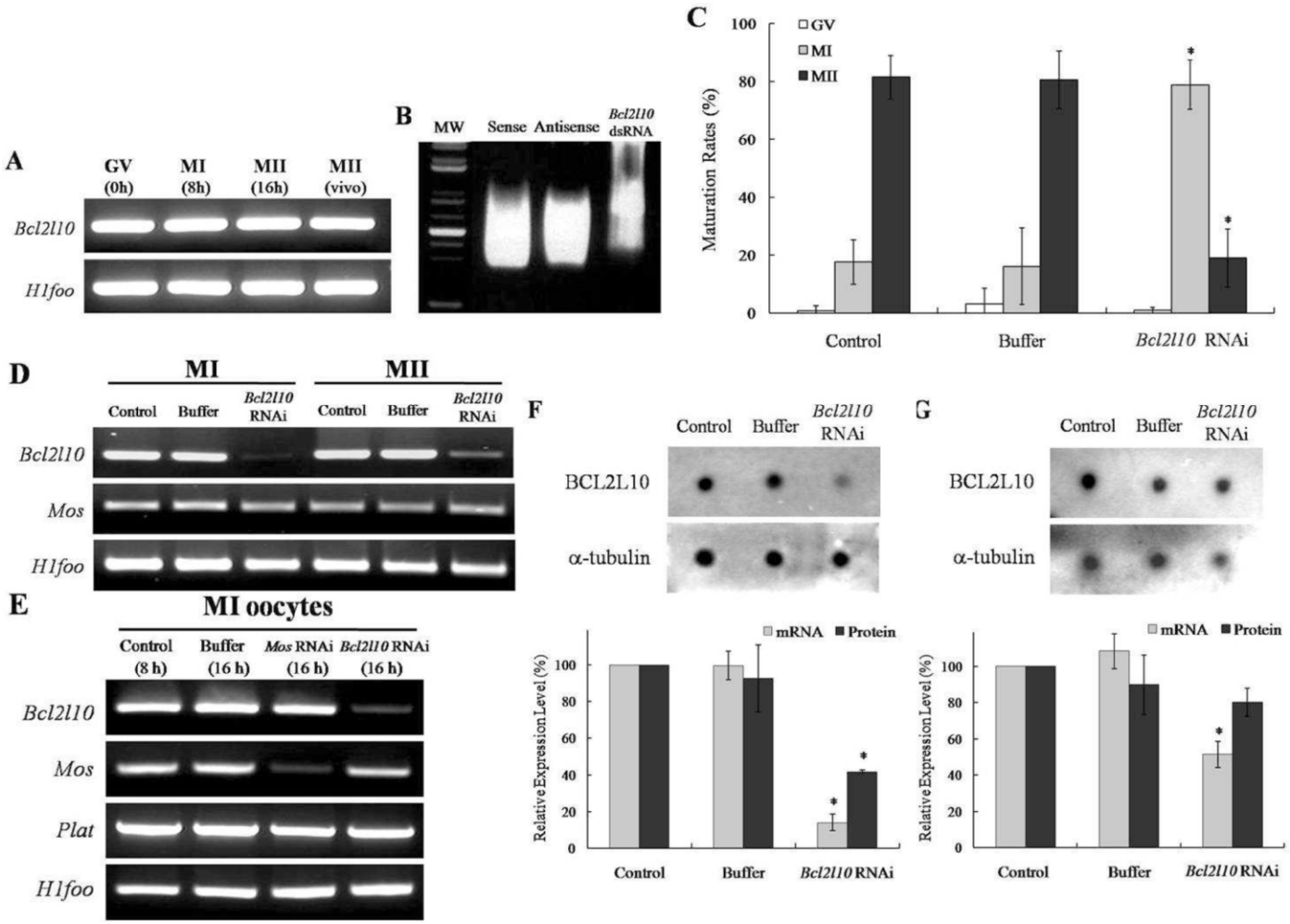

FIG. 4. *Bcl2l10* RNAi and spontaneous maturation. **A**) Semiquantitative RT-PCR analysis of *Bcl2l10* expression at normal oocyte maturation in vitro. GV, GV-stage oocytes; MI, MI-stage oocytes collected at 8 h of in vitro culture; MII, MII oocytes at 16 h; MII vivo, MII oocytes collected directly from mouse oviducts. **B**) Microphotograph showing sense, antisense, and annealed dsRNA for making *Bcl2l10* dsRNA. MW, molecular weight marker. **C**) Microinjection of *Bcl2l10* dsRNA into the GV cytoplasm resulted in most oocytes being arrested at MI. **D**) *Bcl2l10* RNAi effects specific suppression of *Bcl2l10* mRNA expression. Analysis by RT-PCR was used to determine mRNA levels in a single oocyte. After microinjection of *Bcl2l10* dsRNA, expression of untargeted genes (*Mos* and *H1foo*) appears to be unchanged, suggesting *Bcl2l10*-specific silencing. **E**) Confirmation of target gene-specific RNAi effects by using *Bcl2l10* RNAi and *Mos* RNAi to show *Bcl2l10*- and *Mos*-specific decreases, respectively. **F** and **G**) Protein levels in oocytes were determined using dot blot analysis. Proteins were extracted from three MI (**F**) and MII (**G**) oocytes for each dot. *Bcl2l10* mRNA and protein expression after *Bcl2l10* RNAi in the GV oocytes were calculated, and relative expression was analyzed. *$P < 0.05$.

further that the effects of *Bcl2l10* RNAi are *Bcl2l10* specific (Fig. 4E). The RNAi effects on target mRNA expression were measured. In addition to *Mos*, *Bcl2l10*, and *H1foo*, *Plat* was used as another internal control whose sequence does not correspond to either *Mos* or *Bcl2l10* RNAi. As depicted in Figure 4E, *Bcl2l10* RNAi decreased *Bcl2l10* but not *Mos*, whereas *Mos* RNAi decreased *Mos* mRNA only but not *Bcl2l10* and the other genes, *H1foo* and *Plat*, indicating that gene-specific RNAi is working in our system. We confirmed a marked decrease in BCL2L10 protein expression in MI-arrested oocytes after *Bcl2l10* RNAi (Fig. 4F). In the case of MII-developed oocytes after *Bcl2l10* RNAi, oocytes had a lesser decrease in BCL2L10 protein expression compared with that of MI (Fig. 4G). Interestingly, we observed a decrease in tubulin expression in *Bcl2l10* RNAi MII oocytes (Fig. 4G).

When we cultured microinjected oocytes in IBMX-supplemented medium for 24 h to allow oocytes sufficient time to process dsRNA into short interfering RNA while maintaining

TABLE 3. Spindle observation using Pol-Scope imaging in MI and MII oocytes after *Bcl2l10* RNAi.

	No. of MI-developed oocytes (%)			No. of MII-developed oocytes (%)		
Treatment	MI/Total	With spindle	Without spindle	MII/total	With spindle	Without spindle
Control	32/178	32 (100)	0 (0)	144/178	144 (100)	0 (0)
Buffer	36/171	36 (100)	0 (0)	133/171	133 (100)	0 (0)
Bcl2l10 dsRNA	166/213	134 (80.7)*	32 (19.3)*	45/213	45 (100)	0 (0)

* Values are statistical significance at $P < 0.05$.

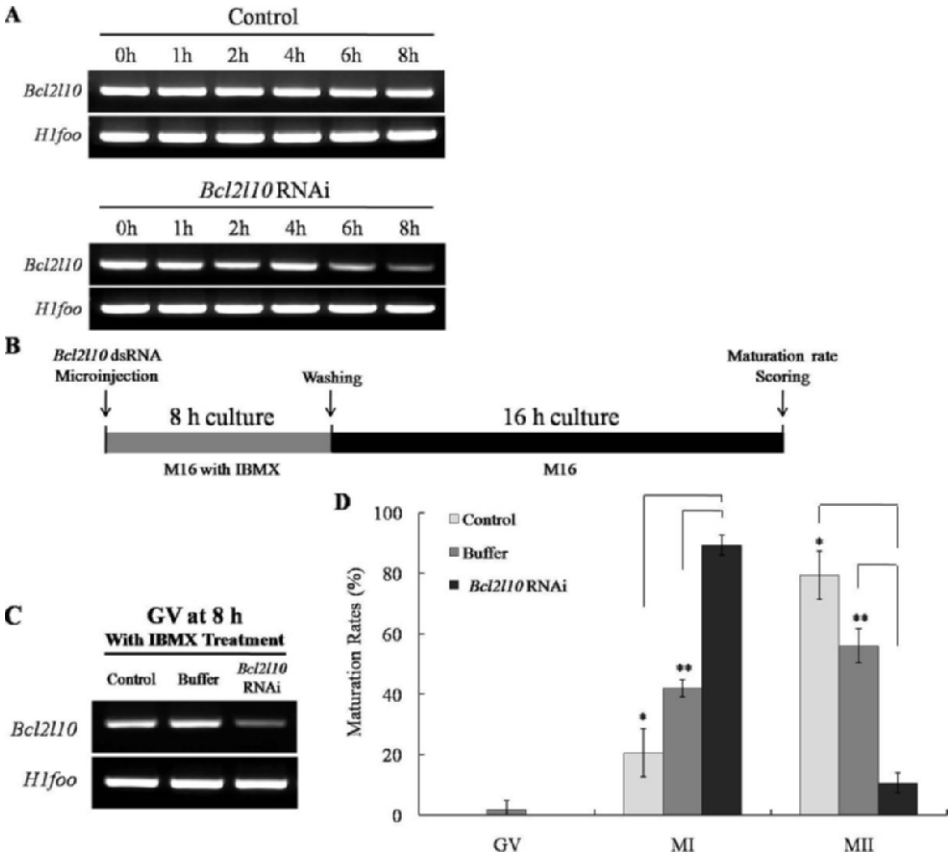

FIG. 5. RNA interference for *Bcl2l10* and spontaneous maturation after GV arrest by IMBX for 8 h. **A**) Typical pattern of *Bcl2l10* mRNA expression during normal in vitro maturation (upper blots) and after *Bcl2l10* RNAi (lower blots). **B**) Diagram for experimental strategy. The GV oocytes were microinjected with *Bcl2l10* dsRNA and cultured in M16 supplemented with IBMX for 8 h, followed by additional 16-h culture in the plain M16. **C**) *Bcl2l10* RNAi and 8-h culture in IBMX medium resulted in specific suppression of *Bcl2l10* mRNA expression at the GV stage. **D**) Maturation rate of oocytes after preincubation in IBMX medium for 8 h, followed by 16-h culture in plain M16 medium. $*P < 0.05$; $**P > 0.05$.

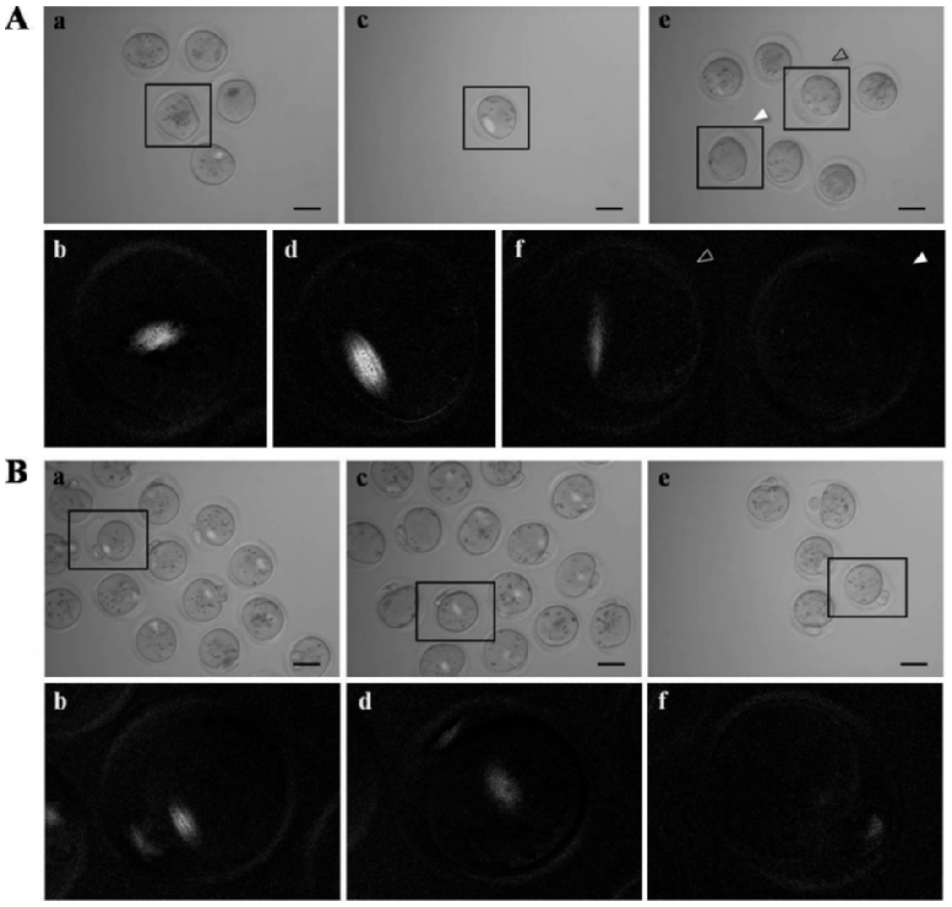

FIG. 6. Noninvasive observation of the spindle structure in live oocytes using PolScope after *Bcl2l10* RNAi. Microphotographs of MI (**A**) and MII (**B**) oocytes cultured in vitro for 16 h after injection of *Bcl2l10* dsRNA, showing the oocytes under the bright field (upper rows) and the dark field in a higher magnification of a representative oocyte in a box (lower rows). **a** and **b**) Control oocytes cultured without any treatment. **c** and **d**) Buffer-injected sham control oocytes. **e** and **f**) *Bcl2l10* dsRNA-injected oocytes. In **Ae** and **Af**, the open arrowhead indicates oocyte with spindle, and the closed arrowhead indicates oocyte without spindle. Original magnifications ×200 (**a**, **c**, and **e**). Bars = 100 μm.

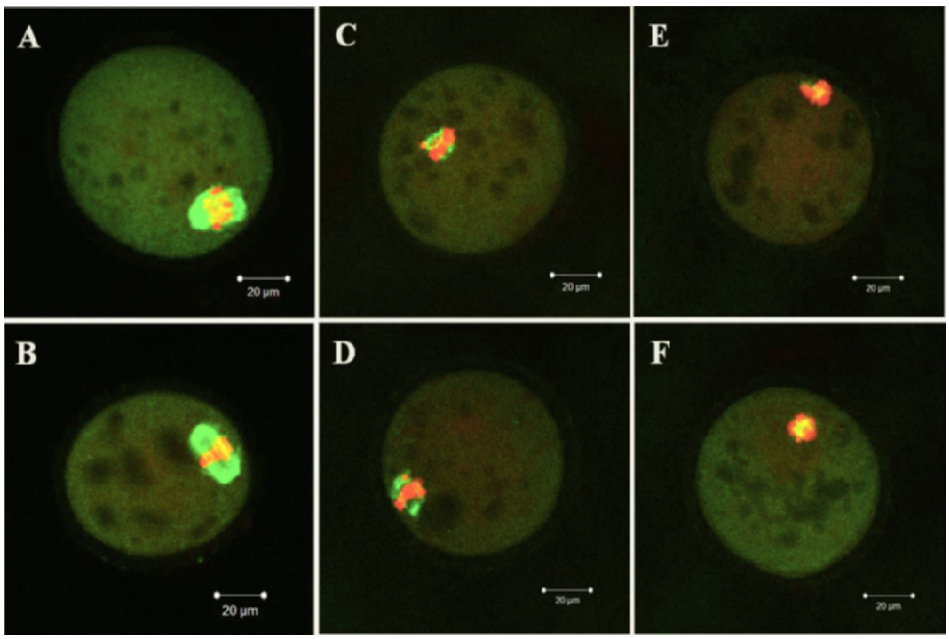

FIG. 7. Immunofluorescence staining of α-tubulin and chromosomes in MI oocytes injected with *Bcl2l10* dsRNA at the immature GV oocyte stage and then cultured for 16 h in vitro. Oocytes were fixed in 4% paraformaldehyde and then stained with an α-tubulin antibody (green). Chromosome material was counterstained with propidium iodide (red). **A**) Control, uninjected oocyte. **B**) Buffer-injected sham control oocytes. **C**–**F**) *Bcl2l10* dsRNA-injected oocytes arrested at the MI stage. Bars = 20 μm.

the GV stage, oocytes kept normal GV. However, most oocytes could not survive the treatment of 24 h of IBMX prior to the 16 h of in vitro maturation in the plain culture medium (data not shown). Therefore, we measured the time period required for degradation of endogenous *Bcl2l10* mRNA (Fig. 5A) and shortened the IBMX treatment duration to 8 h prior to in vitro maturation (Fig. 5B). *Bcl2l10* mRNA decreased in oocytes with *Bcl2l10* RNAi while they maintained GV in IBMX-supplemented medium for 8 h (Fig. 5C). We could not afford further complete knockdown because dsRNA concentration was already high (2 μg/μl), and a longer time of incubation will affect the survival of microinjected oocytes. Preincubation with IBMX showed damaging effects in the buffer-injected group, with increased MI arrest, even though it was not statistically significant (MI, 42%; MII, 56%; $P = 0.07$; Fig. 5D). Nevertheless, when GV oocytes incubated for 8 h in IBMX with *Bcl2l10* RNAi were placed in plain medium, oocytes still started GV breakdown but could not complete meiosis and arrested at MI (89.3%).

We observed oocytes noninvasively and found that *Bcl2l10* RNAi caused abnormalities in the spindle structure of the MI and MII oocytes (Fig. 6). The MI-arrested oocytes exhibited thinner, longer, and weaker spindles (Fig. 6A, e and f, open arrowhead), and no spindle was observed in 19.3% of the oocytes (Fig. 6A, e and f, closed arrowhead; and Table 3). We observed spindles dimly in all MII oocytes after RNAi under Pol-Scope, but they became insubstantial or undetectable when taken as microphotographs (Fig. 6B, f) compared with the barrel shape of spindles in control oocytes (Fig. 6B, b and d).

Changes in the spindle structure and the inferred changes in chromosome configuration were confirmed by immunofluorescence staining. Figure 7 shows microphotographs of MI-arrested oocytes after *Bcl2l10* RNAi taken after immunofluorescence staining. Compared with the fine, healthy, barrel-shaped spindles in the control and buffer-injected oocytes (Fig. 7, A and B), spindles dwindled away (Fig. 7, C and D) or disappeared (Fig. 7, E and F) after *Bcl2l10* RNAi. Chromosomes also aggregated in oocytes with or without spindle

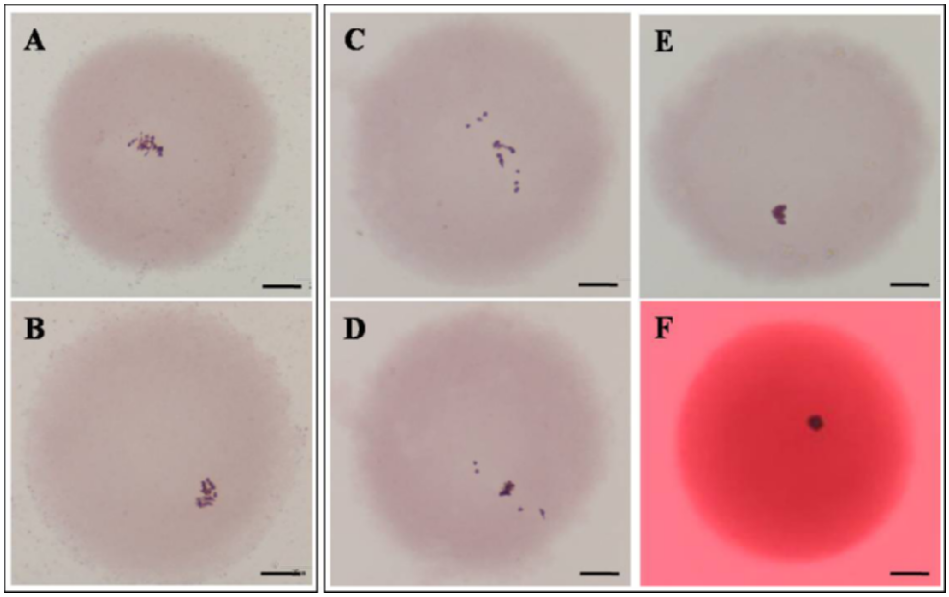

FIG. 8. Chromosomal configuration of MI-arrested oocytes after *Bcl2l10* RNAi by aceto-orcein staining. **A**) Control, uninjected oocyte. **B**) Buffer-injected sham control oocytes. **C** and **D**) *Bcl2l10* dsRNA-injected oocyte, arrested at the MI stage after 16-h culture in vitro, but with a spindle structure. **E** and **F**) *Bcl2l10* dsRNA-injected oocyte, arrested at the MI stage after 16-h culture in vitro, but without a spindle structure. Bars = 25 μm.

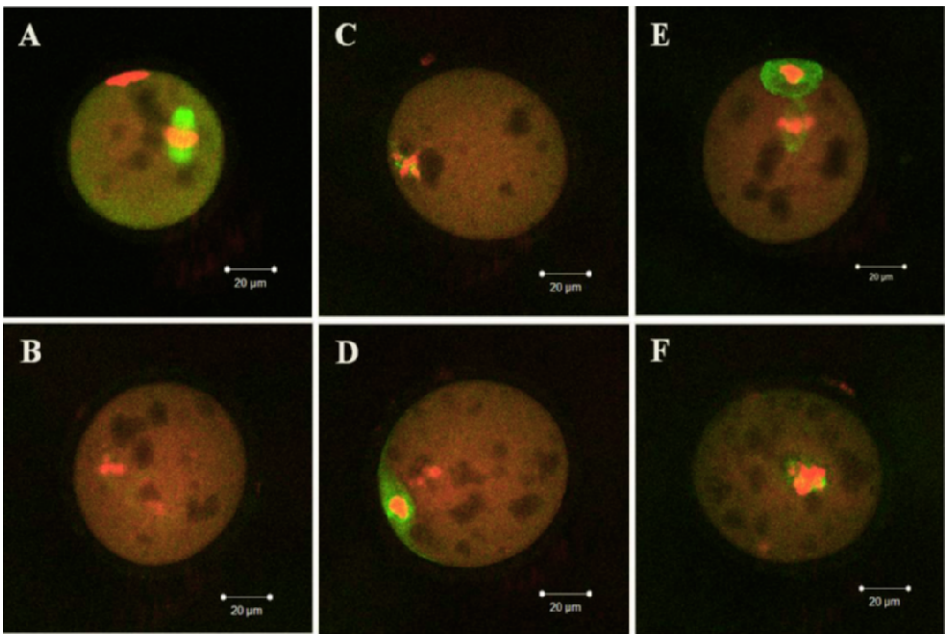

FIG. 9. Immunofluorescence staining of α-tubulin and chromosomes in MII-stage oocytes injected with *Bcl2l10* dsRNA at the immature GV oocyte stage and then cultured for 16 h in vitro. Oocytes were fixed in 4% paraformaldehyde and then stained with a α-tubulin antibody (green). Chromosome material was counterstained with propidium iodide (red). **A**) Control MII oocyte. **B–F**) *Bcl2l10* dsRNA-injected, developed to MII-stage oocytes. Bars = 20 μm.

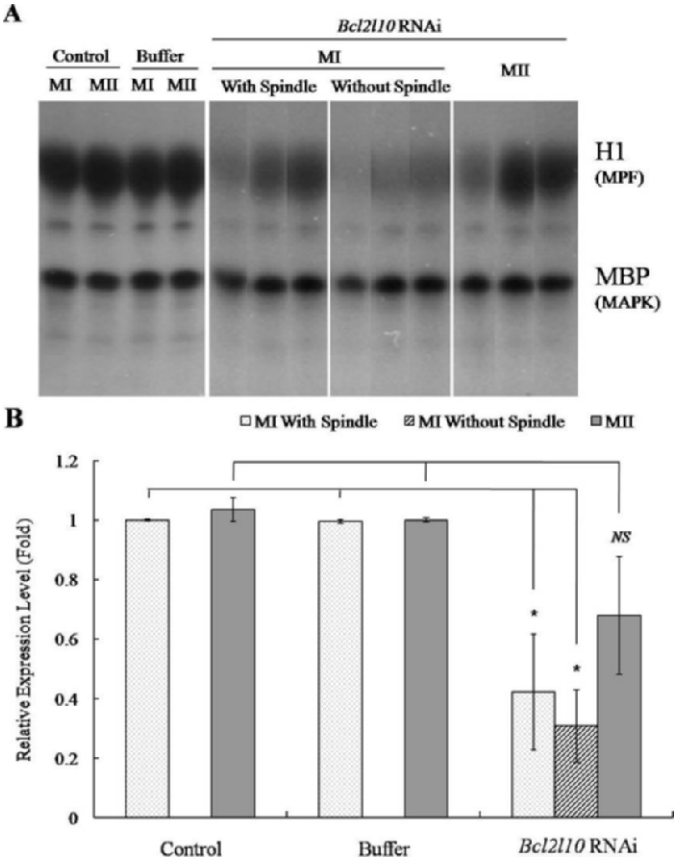

FIG. 10. Dual kinase activity assay. **A**) Phosphorylation of the substrates histone H1 for MPF and MBP for MAPK reflects the activities of these appropriate kinases. Each lane contains one oocyte at each stage, as indicated. Lanes 1–2, control MI and MII; lanes 3–4, buffer-injected MI and MII, lanes 5–7, *Bcl2l10* dsRNA-injected oocyte arrested at the MI stage with spindle structure; lanes 8–10, *Bcl2l10* dsRNA-injected oocyte arrested at the MI stage without spindle structure; lanes 11–13, *Bcl2l10* dsRNA-injected oocyte that developed to the MII stage with a polar body. **B**) Bar graphs indicate mean ± SEM calculated after measuring the area of phosphorylation of the substrates. NS, not significant. $^*P < 0.05$.

remnants (Fig. 7, C–F). Such abnormalities in chromosomal status were verified again by aceto-orcein staining (Fig. 8). Figure 8, A and B, shows the chromosomal shape in normal MI oocytes. Chromosomes were scattered or stretched in MI-arrested oocytes with the spindle (Fig. 8, C and D), whereas all of the chromosomes condensed in a mass in MI-arrested oocytes without a spindle (Fig. 8, E and F).

Approximately 19% of the oocytes developed up to the MII stage regardless of *Bcl2l10* RNAi and appeared normal, with normal size and shape of polar bodies; however, these MII oocytes also exhibited abnormal spindle and chromosome configurations (Fig. 9). All oocytes (Fig. 9) had a normal appearance with polar bodies under light microscopy; however, these MII oocytes with *Bcl2l10* RNAi had severely changed spindles and chromosomes (Fig. 9, B–F).

After finding abnormalities in spindles and chromosomes, we decided to evaluate changes in two well-known regulators of oocyte maturation: MPF and MAPK. We found that MPF activity, but not that of MAPK, was affected by *Bcl2l10* RNAi (Fig. 10A). Activity of these two kinases was assessed after *Bcl2l10* RNAi by measuring the amount of phosphorylation of histone H1 and MBP, substrates of MPF and MAPK, respectively (Fig. 10B). Oocytes that developed to the MII stage despite the *Bcl2l10* knockdown (Fig. 10A, lanes 11–13) had higher MPF activity than MI-arrested oocytes (lanes 5–10) but less than that of control MII oocytes (lanes 1–4).

DISCUSSION

In this study, we confirmed that *Bcl2l10* expression is ovary and oocyte specific. We also found that *Bcl2l10* RNAi caused abnormalities in spindle formation and chromosome segregation, with a concurrent decrease in MPF activity in mouse oocytes matured in vitro. *Bcl2l10* played a noticeable role in completing meiosis in oocytes, particularly at the MI–MII transition.

Results regarding the spatial and temporal distribution of *Bcl2l10* have been very controversial [5, 6, 11, 12]. In this study, we found that *Bcl2l10* mRNA was detected only in ovaries by Northern blotting. No signal was found in any other tissue. However, when RT-PCR was performed, we detected a small amount of *Bcl2l10* mRNA in the epididymis (data not shown).

This is consistent with a previous report showing restricted detection of *Bcl2l10* mRNA in both the ovary and the epididymis [5]. Oocyte-specific expression of *Bcl2l10* is inconsistent with a previous report describing the expression of *Bcl2l10* mRNA in the granulosa cells of the ovary, but not in oocytes [6].

Several antiapoptotic *Bcl2* homologs, including *Bcl2l10*, are expressed in the ovary. *Mcl1*, *Bcl2*, *Bcl2l1* (*Bcl-x*), and other *Bcl2* family members have also been detected in ovarian tissues [13–16]. However, the ovary- and oocyte-specific expression of *Bcl2l10* is quite different from that of other *Bcl2* family members. Murine *Bcl2l10* was first identified in expressed sequence tag clones from unfertilized, fertilized, and two-cell stage mouse eggs [5, 6]. This is consistent with our real-time RT-PCR detection of *Bcl2l10* mRNA in oocytes (GV and MII), pronucleus one-cell zygotes, and two-cell embryos.

After *Bcl2l10* RNAi, the most prominent changes were found in the spindle and chromosome configurations. Spindles of MI oocytes became thinner and longer, and they disappeared in some oocytes. MII oocytes that completed the second meiotic cell cycle with polar body formation (19.1%) even after *Bcl2l10* RNAi still exhibited abnormalities in their spindle and chromosome structures. Noninvasive observation of spindle structure prior to fixation for staining or freezing for measuring RNA expression is useful to get insight into any RNAi effect. Even though the outward appearance of MI or MII oocytes seems normal, we could find that the spindle structure was abnormal when observed noninvasively. Not only did it provide us with the moment in time to decide the next step in how to confirm the effects, but it also gave us the precious oocyte samples for further experiments.

The presence of MI and MII oocytes after RNAi implied that the knockdown effects of *Bcl2l10* mRNA occurred to different extents. We proposed this threshold effect previously [9]. In this experiment, microinjection was performed routinely by a single investigator (E.-Y.K.) using a single automatic microinjector; however, we observed variations among oocytes. Differences between oocytes may be due to the presence of varying levels of *Bcl2l10* mRNA. Loss of *Bcl2l10* mRNA at dissimilar levels, from complete knockdown to only a small reduction, may cause different levels of severity in spindle and chromosome abnormalities. Oocytes with an intermediate *Bcl2l10* mRNA status may exhibit spindle remnants with intermediary chromosome aggregation, whereas oocytes with a small degree of knockdown in *Bcl2l10* mRNA could complete meiosis to become MII oocytes. Gradual reduction of mRNA (Fig. 4D), protein (Fig. 4, F and G), and MPF activity (Fig. 10) support this threshold proposition.

It was interesting to find the reduction of tubulin expression that we used as an internal control for oocyte dot blot, a modified Western blot. If we consider the abnormalities observed in spindle structure after *Bcl2l10* RNAi, we can take the reduction in the amount of tubulin expression as a reasonable outcome related to disappearance of the spindle structure. For that reason, we could not use tubulin expression as a control for normalization in the case of MII oocytes (Fig. 4G). We found gradual reduction in *Tuba1* (α-tubulin) mRNA (i.e., less in MI and more in MII; data not shown) that match with protein expression. Further research on the association of BCL2L10 with spindle formation is necessary.

It was exciting to find that a reduction in intracellular *Bcl2l10* expression during oocyte maturation caused changes in MPF activity but not MAPK activity. It is not clear whether changes in MPF activity were due to a direct or indirect effect of *Bcl2l10* RNAi; however, it is tempting to conclude that there is a network among BCL2L10 or BCL2L10-related proteins, spindles, and MPF. We assume that the disorganized spindle structure that was present after *Bcl2l10* RNAi may cause this change in MPF activity. Components of MPF are closely related to the spindle structure. It has been reported that cyclin B1 and phosphorylated cyclin B1 are localized around condensed chromosomes and concentrated at the spindle poles, whereas CDC2 (p34) is localized in the spindle region during spindle formation at metaphase I [17].

An alternative explanation for these results is also possible: changes in MPF induced by *Bcl2l10* RNAi through a not-yet-known mechanism may induce abnormalities in the spindle. Indeed, it has been reported that the transition of microtubule dynamics is induced by phosphorylation reactions mediated by MPF [18] and MAPK [19] functioning downstream of MPF [20].

It was interesting to determine that *Bcl2l10* RNAi had no effect on the MAPK cascade. We used the expression of *H1foo* and *Mos* as internal controls to illustrate that microinjected dsRNA affected a sequence-specific target only. *H1foo* is a well-known housekeeping gene, and *Mos* is the first gene that was studied using RNAi [9, 10]. At the same time, *Mos* functions upstream of MAPK signaling cascades [21]; thus, we can conclude that *Bcl2l10* RNAi does not appear to regulate MAPK signaling cascades upstream of Mos or MAPK itself.

Previous studies have suggested that complicated relationships exist between MAPK and MPF pathways. MAPK activation may regulate proteins that control MPF activity directly or indirectly, including CDC25 phosphatase, WEE1 kinase, and MYT1 kinase [22–24]. *Myt1* is regulated by the MAPK substrate, RPS6KA (Rsk), or MOS, providing a connection between MOS/MAPK and MPF activation [25, 26]. In contrast, MPF has also been implicated in the activation of MAPKs [20, 27]. Recently, it has been reported that CDC2 activation in *Xenopus* oocytes, either by cyclin B or MOSXE (Mos), is required for inducing meiotic maturation; these two pathways appear to be functionally redundant [27]. Further investigation into the correlation between MPF, MAPK, and BCL2L10 in mouse oocyte maturation is required.

In conclusion, this is the first report on the function of BCL2L10 that is related to the regulation of meiosis and intracellular structures in mouse oocytes. Further studies will be required to determine the details of the molecular mechanisms that exist among BCL2L10 and BCL2L10-related working partners and the cellular features of oocytes in meiosis completion.

REFERENCES

1. DeJong J. Basic mechanisms for the control of germ cell gene expression. Gene 2006; 366:39–50.
2. Yoon SJ, Chung HM, Cha KY, Kim NH, Lee KA. Identification of differential gene expression in germinal vesicle vs. metaphase II mouse oocytes by using annealing control primers. Fertil Steril 2005; 83(suppl 1): 1293–1296.
3. Yoon SJ, Koo DB, Park JS, Choi KH, Han YM, Lee KA. Role of cytosolic malate dehydrogenase in oocyte maturation and embryo development. Fertil Steril 2006; 86(suppl 4):1129–1136.
4. Kim KH, Kim EY, Lee KA. SEBOX is essential for early embryogenesis at the two-cell stage in the mouse. Biol Reprod 2008; 79:1192–1201.
5. Song Q, Kuang Y, Dixit VM, Vincenz C. Boo, a novel negative regulator of cell death, interacts with Apaf-1. EMBO J 1999; 18:167–178.
6. Inohara N, Gourley TS, Carrio R, Muñiz M, Merino J, Garcia I, Koseki T, Hu Y, Chen S, Núñez G. Diva, a Bcl-2 homologue that binds directly to Apaf-1 and induces BH3-independent cell death. J Biol Chem 1998; 273: 32479–32486.
7. Kim JH, Yoon S, Won M, Sim SH, Ko JJ, Han S, Lee KA, Lee K, Bae J. HIP1R interacts with a member of Bcl-2 family, BCL2L10, and induces BAK-dependent cell death. Cell Physiol Biochem 2009; 23:43–52.
8. McGrath SA, Esquela AF, Lee SJ. Oocyte-specific expression of growth/differentiation factor-9. Mol Endocrinol 1995; 9:131–136.
9. Park CE, Shin MR, Jeon EH, Lee SH, Cha KY, Kim K, Kim NH, Lee KA.

Oocyte-selective expression of MT transposon-like element, clone MTi7 and its role in oocyte maturation and embryo development. Mol Reprod Dev 2004; 69:365–374.
10. Svoboda P, Stein P, Hayashi H, Schultz RM. Selective reduction of dormant maternal mRNAs in mouse oocytes by RNA interference. Development 2000; 127:4147–4156.
11. Ke N, Godzik A, Reed JC. Bcl-B, a novel Bcl-2 family member that differentially binds and regulates Bax and Bak. J Biol Chem 2001; 276: 12481–12484.
12. Lee R, Chen J, Matthews CP, McDougall JK, Neiman PE. Characterization of NR13-related human cell death regulator, Boo/Diva, in normal and cancer tissues. Biochim Biophys Acta 2001; 1520:187–194.
13. Tilly JL, Tilly KI, Kenton ML, Johnson AL. Expression of members of the bcl-2 gene family in the immature rat ovary: equine chorionic gonadotropin-mediated inhibition of granulosa cell apoptosis is associated with decreased bax and constitutive bcl-2 and bcl-xlong messenger ribonucleic acid levels. Endocrinology 1995; 136:232–241.
14. Hsu SY, Kaipia A, McGee E, Lomeli M, Hsueh AJ. Bok is a pro-apoptotic Bcl-2 protein with restricted expression in reproductive tissues and heterodimerizes with selective anti-apoptotic Bcl-2 family members. Proc Natl Acad Sci U S A 1997; 94:12401–12406.
15. Hsu SY, Hsueh AJ. Tissue-specific Bcl-2 protein partners in apoptosis: an ovarian paradigm. Physiol Rev 2000; 80:593–614.
16. Kim MR, Tilly JL. Current concepts in Bcl-2 family member regulation of female germ cell development and survival. Biochim Biophys Acta 2004; 1644:205–210.
17. Huo LJ, Yu LZ, Liang CG, Fan HY, Chen DY, Sun QY. Cell-cycle-dependent subcellular localization of cyclin B1, phosphorylated cyclin B1 and p34cdc2 during oocyte meiotic maturation and fertilization in mouse. Zygote 2005; 13:45–53.
18. Verde F, Labbé JC, Dorée M, Karsenti E. Regulation of microtubule dynamics by cdc2 protein kinase in cell-free extracts of *Xenopus* eggs. Nature 1990; 343:233–238.
19. Gotoh Y, Nishida E, Matsuda S, Shiina N, Kosako H, Shiokawa K, Akiyama T, Ohta K, Sakai H. In vitro effects on microtubule dynamics of purified *Xenopus* M phase-activated MAP kinase. Nature 1991; 349:251–254.
20. Gotoh Y, Moriyama K, Matsuda S, Okumura E, Kishimoto T, Kawasaki H, Suzuki K, Yahara I, Sakai H, Nishida E. *Xenopus* M phase MAP kinase: isolation of its cDNA and activation by MPF. EMBO J 1991; 10: 2661–2668.
21. Verlhac MH, Lefebvre C, Guillaud P, Rassinier P, Maro B. Asymmetric division in mouse oocytes: with or without Mos. Curr Biol 2000; 10:1303–1306.
22. Huang CY, Ferrell JE Jr. Dependence of Mos-induced Cdc2 activation of MAP kinase function in a cell-free system. EMBO J 1996; 15:2169–2173.
23. Abireu A, Dorée M, Picard A. Mitogen-activated protein kinase activation down-regulates a mechanism that inactivates cyclin B-cdc2 kinase in G2-arrested oocytes. Mol Biol Cell 1997; 8:249–261.
24. Palmer A, Gavin AC, Nebreda AR. A link between MAP kinase and p34(cdc2)/cyclin B during oocyte maturation: p90(rsk) phosphorylates and inactivates the p34(cdc2) inhibitory kinase Myt1. EMBO J 1998; 17: 5037–5047.
25. Peter M, Labbe JC, Doree M, Mandart E. A new role for Mos in *Xenopus* oocyte maturation: targeting Myt1 independently of MAPK. Development 2002; 129:2129–2139.
26. Haccard O, Jessus C, Rime H, Goris J, Merlevede W, Ozen R. Mitogen-activated protein kinase (MAP kinase) activation in *Xenopus* oocytes: roles of MPF and protein synthesis. Mol Reprod Dev 1993; 36:96–105.
27. Haccard O, Jessus C. Redundant pathways for Cdc2 activation in *Xenopus* oocyte: either cyclin B or Mos synthesis. EMBO Rep 2006; 7:321–325.